Validation of the CAVEMAN Human Body Model Lumbar Spine Response to Vertical Accelerative Loading and the Effect of Spine Curvature on Skeletal Fracture.

Kent D. Butz, Chad M. Spurlock, Kevin Lister

Abstract The aim of this study was to evaluate the biofidelity of the CAVEMAN human body model lumbar spine and to evaluate the effects of variation in lumbar spine posture on load transmission and injury location. The CAVEMAN model was validated against vertical impact experiments at sub-injurious loading rates using data sets derived from post-mortem human subject testing. The spine model was positioned to represent the curvature of six post-mortem human subject spines, and each posture model was then loaded vertically with identical input conditions. These simulations were then repeated at an injurious loading rate, and the predicted fracture locations and severity were compared. The load response of the CAVEMAN spine models were found to be within the measured range of the post-mortem human subject response and within ±1 standard deviation of the mean response through the time of peak impact. The magnitude of peak load measured in the models, as well as predicted fracture locations and severities, were dependent on spine posture, with sacrum angle the predominant factor.

Keywords CAVEMAN, computational modelling, finite element modelling, injury biomechanics, spine injury

I. INTRODUCTION

The ability to accurately predict spinal injury resulting from high acceleration loading has become an area of focus in recent years for the U.S. military when confronting the use of improvised explosive devices (IEDs) abroad. In the past two decades, the use of IEDs in the conflicts in Iraq and Afghanistan has led to numerous injuries and deaths caused by underbody blast (UBB) events. Such UBB events can lead to high acceleration impacts to the lumbar spine, raising an increased need to understand the biomechanical response of the spine to such loads in the effort to produce better protective equipment and safer vehicular design.

In order to address these objectives, the U.S. military has been using the Hybrid III 50th percentile male anthropomorphic test device (ATD) to gauge injury risk in vehicular UBB testing. However, these devices are limited to the evaluation of a subset of skeletal injuries and cannot provide insight into the potential for damage incurred in the surrounding soft tissue. Further, because the Hybrid III was designed for application in automotive crash analysis rather than military applications, the ATD does not correlate well to human injury responses in alternative loading situations, such as vertical underbody loading, as has been demonstrated in analyses of lower limb injury surrogates [1].

Human finite element models can address these issues through full representation of the human anatomy, including the soft tissue, and several computational models have been developed over the last several years in an effort to improve biomechanical analysis and injury prediction. One such model includes the Total Human Model for Safety (THUMS), developed by Toyota Motor Corporation for application in the automotive industry but has also been applied to a variety of impact and injury models [2–5]. Similarly, the whole body model of the Global Human Body Models Consortium (GHBMC) is another example of a full body computational model used in the analysis of civilian automotive events and numerous other research applications [6-7]. In addition to these full body models, computational models of the isolated lumbar spine have been generated by numerous research groups to study a range of issues related to spine biomechanics including disc mechanics and degeneration [8–10], soft tissue response [11], the biomechanical response to compression and bending of the lumbar spine [12–15], and the influence of spine curvature on load distribution [16].

K. D. Butz (+1 704-799-6944; kent.butz@corvidtec.com), C. M. Spurlock, and K. Lister are Computational Analysists at Corvid Technologies, LLC, Mooresville, NC, USA.

The Computational Anthropomorphic Virtual Experiment Man (CAVEMAN) finite element human body model is being developed by Corvid Technologies as an analysis tool to improve injury analysis capabilities for both skeletal and soft tissues across a broad range of applications and loading rates. The CAVEMAN human body model is a highly detailed finite element model based upon the geometry of the Zygote 50th percentile male human body. The anatomy for the human body model was developed by Zygote Media Group using computed tomography (CT) and magnetic resonance imaging (MRI) scans, and the musculoskeletal anatomy used in the full CAVEMAN model consists of the full skeleton, 397 muscles, 342 ligaments, 16 organs, and skin. This model is being developed for biomechanics analysis and injury prediction and to date has been validated in the analysis of lower leg injury caused by high acceleration loading [17].

However, whether performed physically through the use of ATDs or computationally through the use of finite element models, accurate prediction of injury modalities and severity in a design environment rely upon the experimental data obtained from Post-Mortem Human Subject (PMHS) testing for model validation. These experiments are frequently performed on individual regions of the body, such as the lumbar spine, to isolate the component response. Though PMHS testing is an essential component in developing accurate computational models of the spine, differences across subjects can result in variations within an experimental data set even when parameters such as age and condition are met in PMHS. These variations may in turn affect model validation efforts. One such parameter is curvature within the spine, which may differ between subjects even when the overall angle of the spinal column is consistent. This variation may be due to several factors, for example a PMHS spine may have limitations in the extent to which it can be physically positioned without damaging the surrounding tissue.

The objectives of this study were to validate the CAVEMAN finite element model whole lumbar spine response and to evaluate the effects of variation in lumbar spine curvature on load transmission and predicted injury location. The CAVEMAN lumbar spine was evaluated against PMHS vertical impact experiments at sub-injurious and injurious loading rates using data sets derived from PMHS testing that was performed as part of the Warrior Injury Assessment Manikin (WIAMan) programme. The spine was positioned to six postures simulating variation in lumbar curvature and approximate to the neutral posture definition from the experimental setup [18]. The positioned finite element models were then loaded vertically with identical parameters and inputs. Spine loads were measured from simulated load cells mounted to the upper and lower potting of the spine, and peak loads, as well as the predicted injury characteristics and locations, were then compared across the six postures.

II. METHODS

As part of the U.S. Army's effort to develop the next generation ATD for mounted crew injury evaluation, the WIAMan programme has conducted numerous tests on PMHSs under vertical acceleration loading. The lumbar spine component level test selected for use as a validation data set in the present work was conducted at the Medical College of Wisconsin (MCW) [18-19]. The test configuration was replicated using the CAVEMAN model to evaluate model biofidelity.

In these experiments, the lumbar spine was rigidly potted in polymethyl methacrylate (PMMA) at the sacrum and T12. The T12 vertebra was mounted at a target angle of +5 degrees from horizontal. The target spinal column angle, defined as the angle between the joint centres of T12/L1 and S1/L5 with respect to the vertical axis, was 12 degrees. The potting on both ends of the spine were mounted to load cells which were in turn connected to slides attached to vertical rails [18]. The bottom of the spine was then impacted vertically by an impact plate driven by a drop mass. For the experimental case used, the targeted peak velocity was 1.2 m/s [19].

The lumbar spine model presented in this study is a subset of the CAVEMAN full body model and includes the sacrum, L1-L5, T12, and the associated intervertebral discs spanning each joint segment. The vertebral endplates were not included in this model. Each vertebra and the sacrum were segmented from the scan data to include representations of both the cortical and cancellous bone regions. The thickness of the cortical layer varied throughout the vertebral bodies based upon CT scan data provided by Zygote Media Group. Both cortical and cancellous bone were meshed with solid hexahedral elements, with a minimum of two elements through the thickness of the cortical bone layer. Both regions of the bone were modelled as isotropic, elastic-plastic materials with failure:

$$\boldsymbol{\sigma} = \begin{cases} E\boldsymbol{\varepsilon}, & \|\boldsymbol{\sigma}\| \leq \boldsymbol{\sigma_0} \\ \boldsymbol{\sigma}_0 + \frac{EE_T}{E-E_T}\bar{\boldsymbol{\varepsilon}}^p, & \|\boldsymbol{\sigma}\| > \boldsymbol{\sigma_0} \end{cases}, \quad (1)$$

where $\boldsymbol{\sigma}$ is stress (Pa), E is Young's modulus (Pa), $\boldsymbol{\varepsilon}$ is engineering strain (-), $\boldsymbol{\sigma_0}$ is yield stress (Pa), E_T is the tangent modulus, and $\bar{\boldsymbol{\varepsilon}}^p$ is the effective plastic strain at failure.

The material failure criteria was based on effective plastic strain with the ability to allow element deletion should the failure criteria be met. In the cortical bone, element deletion was active in order to represent fracture of the bone. However, element deletion was not allowed in the cancellous bone. Instead, upon failure, the material model set the element shear stresses to zero and the element became hydrostatic, allowing load transmission to continue through the cancellous region.

The intervertebral discs included separate regions for the nucleus pulposus and annulus fibrosis connected to the vertebral bodies with tied node definitions. The nucleus pulposus was modelled as an isotropic Mooney-Rivlin solid:

$$W = C_1(I_1 - 3) + C_2(I_2 - 3), \quad (2)$$

where W is the strain energy density function, C_1 is the first invariant coefficient, C_2 is the second invariant coefficient, and I_1 and I_2 are the invariants of the right Cauchy-Green tensor.

The annulus fibrosis was modelled as a fibre-reinforced transversely isotropic solid [20]:

$$W = C_1(\tilde{I}_1 - 3) + C_2(\tilde{I}_2 - 3) + \frac{K}{2}(\ln J)^2 + F\langle\lambda\rangle, \quad (3)$$

$$\frac{\partial F}{\partial \lambda} = \begin{cases} \frac{C_3}{\lambda}\left(\exp\left(C_4(\lambda - 1)\right) - 1\right), & \lambda < \lambda^* \\ \frac{1}{\lambda}(C_5\lambda + C_6), & \lambda \geq \lambda^* \end{cases}, \quad (4)$$

where W is the strain energy density function, C_1 is the first invariant coefficient (Pa), C_2 is the second invariant coefficient (Pa), I_1 and I_2 are the invariants of the right Cauchy-Green tensor, K is the bulk modulus (Pa), J is the volume ratio, $F\langle\lambda\rangle$ is the fibre strain term, λ represents fibre stretch along the fibre direction, λ^* is the stretch where the fibres transition from exponential to linear behaviour, C_3 scales the exponential stress (Pa), C_4 controls the rate of uncramping of the fibres, C_5 is the linear modulus of the straightened fibres (Pa), and C_6 ensures continuity between exponential and linear regions of the fibre term.

The fibre component of the annulus fibrosis material model was assumed to be aligned along vectors oriented ± 30 degrees from the plane of the disc in four alternating layers of elements from the outer surface of the disc to the nucleus [21-22].

TABLE I
MATERIAL DEFINITIONS USED IN THE LUMBAR SPINE MODEL.

Material	Component	Coefficients		Ref
Elastic-Plastic	Cortical Bone	$\rho = 1.83\frac{g}{cm^3}$	$\sigma_0 = 110\ MPa$	[14]
		$G = 5.38\ GPa$	$E_T = 4.65\ GPa$	
	Cancellous Bone	$\rho = 0.17\frac{g}{cm^3}$	$\sigma_0 = 1.92\ MPa$	[23]
		$G = 116\ MPa$	$E_T = 21.4\ MPa$	
Mooney-Rivlin	Nucleus Pulposus	$\rho = 1.0\frac{g}{cm^3}$	$C_1 = 120\ kPa$	[14]
		$\nu = 0.495$	$C_2 = 30\ kPa$	

Transversely Isotropic Hyperelastic	Annulus Fibrosus	$C_1 = 0.18\ MPa$ $C_2 = 450\ kPa$ $C_3 = 48.1\ MPa$ $C_4 = 15.13$ $C_5 = 250\ MPa$	$\rho = 1.2\frac{g}{cm^3}$ $K = 0.735\ GPa$ $\lambda^* = 0.35$	[14][24]

The nominal CAVEMAN lumbar segments were positioned to replicate different postures for the lumbar spine (Fig. 1). The parameters used to define the lumbar segment postures were the angle of the individual vertebral bodies, the angle between adjacent joint centres, and the overall spinal column angle as measured from the centre of L1/T12 to S1/L5 (Table 2). All other features of the geometry and material characteristics were held constant, maintaining posture as the parameter driving the variance in model response. The six postures resulted in virtual, subject-specific posture variations approximate to the experimentally defined neutral postures of +5 degree T12 offset and 12 degree column angle.

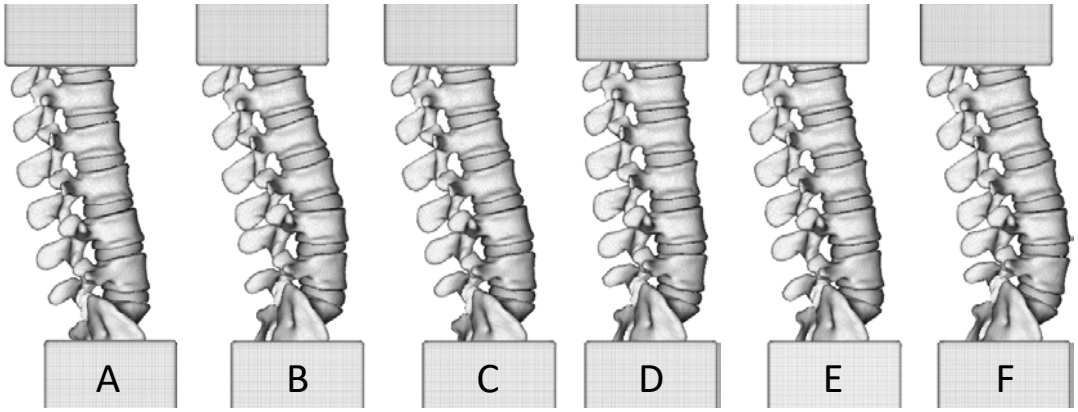

Fig. 1. Side view of the repositioned lumbar spine. Each posture approximates the vertebral and spinal column angle of mounted PMHS spines in the experimental data set used in this work as a validation test case.

TABLE II
SUPERIOR ENDPLATE ANGLE FROM S1 TO L1 FOR EACH POSTURE, MEASURED FROM THE HORIZONTAL PLANE. COLUMN ANGLE IS MEASURED FROM THE CENTRE OF INTERVERTEBRAL DISCS S1/L5 TO L1/T12, MEASURED FROM THE VERTICAL PLANE. ALL ANGLES ARE PRESENTED IN DEGREES.

	Sacrum	L5	L4	L3	L2	L1	Column Angle
Posture A	-4.7	10.5	10.9	7.8	6.5	3.9	9.0
Posture B	-21.8	4.7	3.5	9.0	14.7	11.6	11.3
Posture C	-10.4	5.8	9.3	10.2	11.7	5.6	10.9
Posture D	-20.3	0	6.5	6.5	4.9	1.6	7.4
Posture E	-20.1	7.8	8.4	10.3	11.6	9.1	10.8
Posture F	-26.1	6.2	4.8	9.9	13.6	13.6	9.8

The vertebral bodies were rotated in LS-PrePost about joint centres identified as the centre of the intervertebral discs. The intervertebral discs were then positioned using a custom Python script such that the disc nodes attached to the vertebrae were rotated to maintain contact with the rotated vertebrae, and the rotation of the interior nodes was interpolated such that an equal thickness of the element layers through the height of the disc was achieved. As a validation test case, the CAVEMAN model response was compared against the experimental Biofidelic Response Corridors (BRC) developed from the PMHS response by the WIAMan programme [19]. Across all simulations in this validation test case only the spine posture was modified. The CAVEMAN sacrum and T12 vertebra were virtually mounted in the test rig model with PMMA potting blocks (Fig. 2). The blocks conformed to the bone geometry without interference of the joint space. The sacrum potting was remeshed as necessary to accommodate variations in sacrum angle. The angle of T12 and the associated potting geometry were maintained constant for each test.

The model was run on 32 processors within Velodyne (Version 3.102.02), a massively parallel, explicit, nonlinear finite element solver developed by Corvid Technologies. A typical simulation had a run time of approximately 9 hours with a timestep of 6.5E-08. The model was compared to an experimental data set with a peak velocity of 1.2 m/s [19]. The velocity was used as the model input and applied to the bottom surface of the lower mounting plate. Load cells mounted between the test rig and the upper and lower PMMA potting recorded the loads applied to the system. The CAVEMAN model output to this loading condition was then compared to the experimental output. Following the validation test, the input was then scaled to a peak velocity of 4.8 m/s to induce injury on the six test postures and the location and severity of injury was compared across simulations.

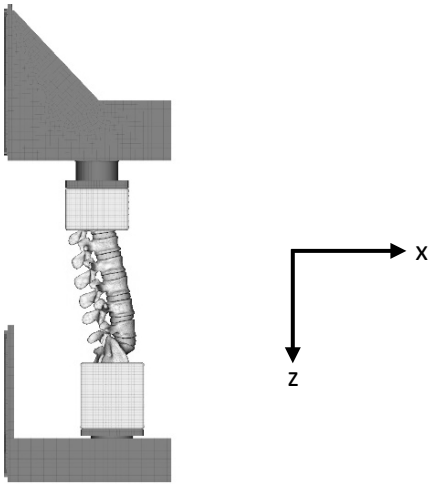

Fig. 2. Overview of the lumbar spine test configuration. The lumbar spine was potted in PMMA blocks attached to the test rig. Load cells positioned between the PMMA and test rig were used to determine lower and upper lumbar force. A velocity input condition was applied to the bottom surface of the rig. Both upper and lower sleds of the rig were free to move vertically along the z-axis, with zero displacement boundary conditions applied in the x and y direction.

III. RESULTS

For the validation test case, five of the six postures (B-F) adhered closely to published lumbar force BRCs in the axial direction through the first 12 ms of loading (Fig. 3a-b). In the latter half of the loading curve, the same five postures maintained a response near the boundary to the ±1 standard deviation corridor of the validation data set. Posture A was an outlier with a much stiffer axial response through the first 16 ms. The load cell response of Posture A in these simulations remained within the ±1 standard deviation corridor through the initial loading, up to 13 ms, before exiting the corridor briefly at peak load. All simulations were observed to exhibit a single-peak response, in contrast with the double peak response of the PMHS validation data. Additional data traces are also presented for all six postures showing the spinal compression as well as lower and upper lumbar forces in the anterior-posterior direction in Fig. 3c-e.

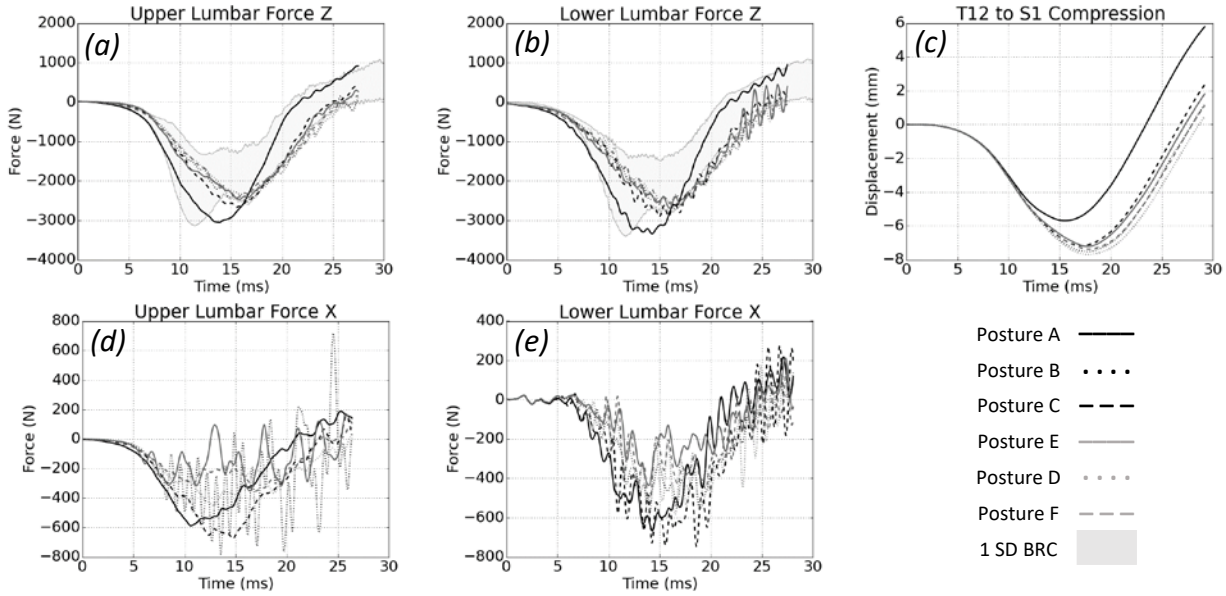

Fig. 3. (a-b) Comparison of the CAVEMAN lumbar spine load cell response in the axial direction for a 1.2 m/s impact across six postures to the PMHS ±1 standard deviation response corridor for the validation data set (light grey) [19]. (c-e) Comparison of total spine compression and load cell off-axis response for the six simulations. In these tests the positive z-axis is oriented downward in the axial direction and the positive x-axis is oriented from the posterior of the spine to the anterior.

The 1.2 m/s test condition resulted in variation in load cell response across the six posture simulations. The load cell response for each simulation is shown in Fig. 3. Posture A had the largest peak force, with a magnitude of 3053 N at the upper load cell and 3344 N at the lower load cell. Across all postures the average peak upper load cell force was 2588 N with a standard deviation of 231 N. Average peak load at the lower load cell was 2797 N with a standard deviation of 270 N. No injuries were predicted for any simulated posture under this test condition.

For the injurious test case (4.8 m/s), the average peak load for the six postures was 5860 N at the upper load cell with a standard deviation of 587 N (Fig. 4). At the lower load cell, the average peak load was 7614 N with a standard deviation of 636 N. Because the simulations terminated at different time points due to fracture-induced failure, predicted injuries were compared at 11 ms which was the termination time of the shortest simulation. Vertebral fracture injuries were predicted to occur in all six simulations and varied across the six postures (Fig. 5). At 11 ms, postures A, B, C, and D each predicted in fractures in L5, propagating from the lower surface of the vertebral body. Posture B resulted in additional fractures to the L3 and L4 spinous processes and a small fracture in L1, while Postures C, D, E, and F predicted burst fractures in L1 (Fig. 6).

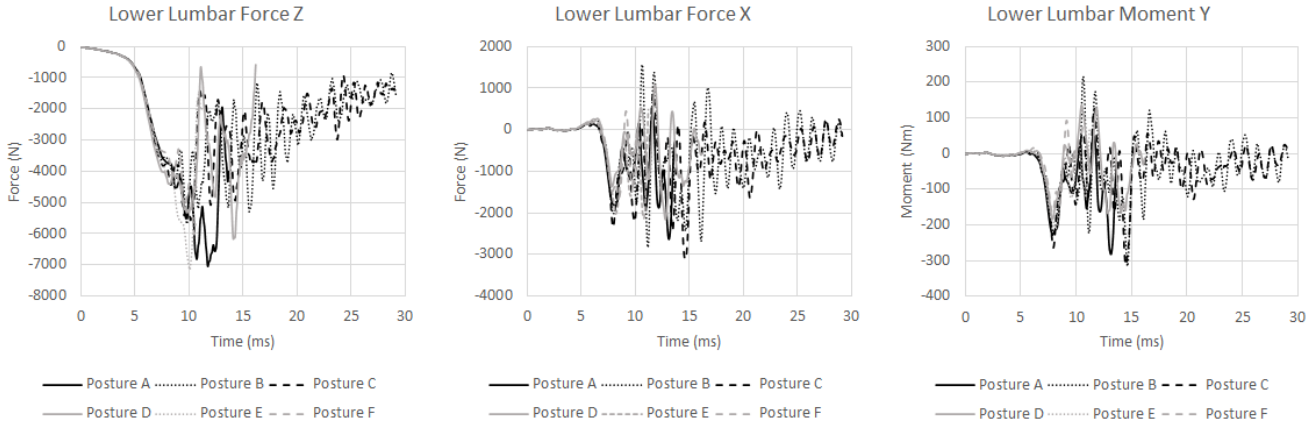

Fig. 4. Comparison of lower load cell forces and moment for an injurious impact condition across the six test postures. Peak input velocity was 4.8 m/s.

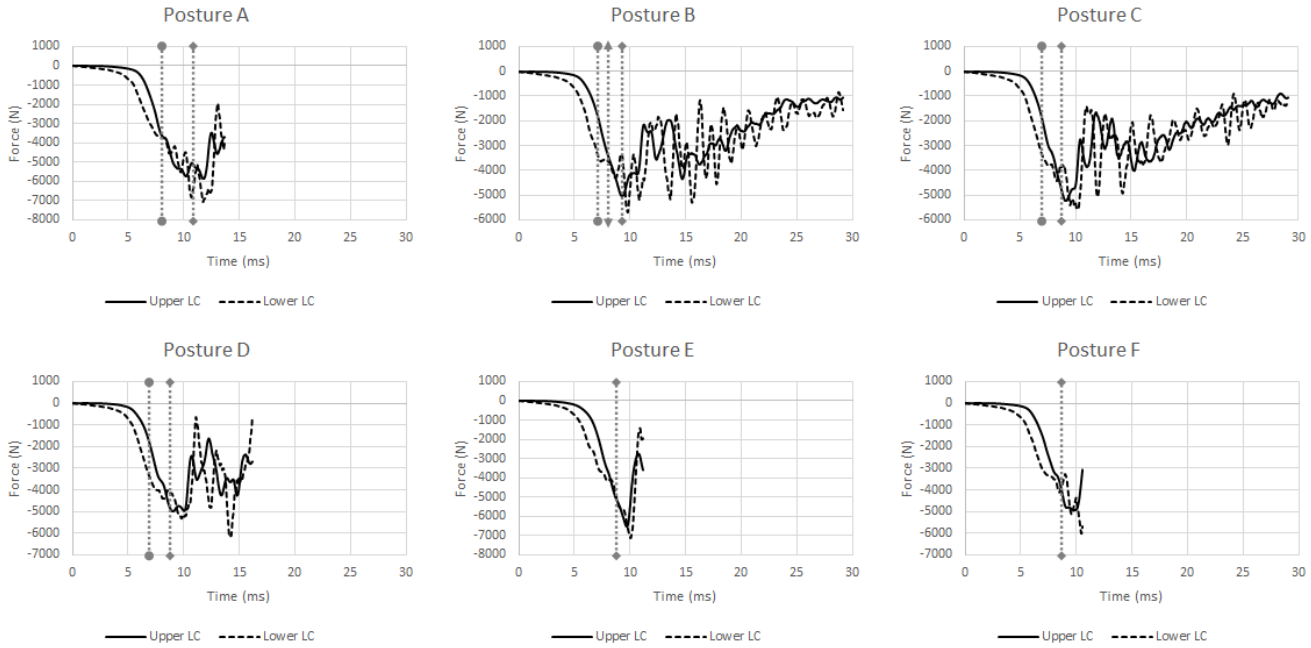

Fig. 5. Comparison of upper and lower load cell response for injurious impact condition across the six test postures. Vertical lines represent the predicted time of fracture (circle = L1 fracture, diamond = L5 fracture, triangle = spinous process fracture).

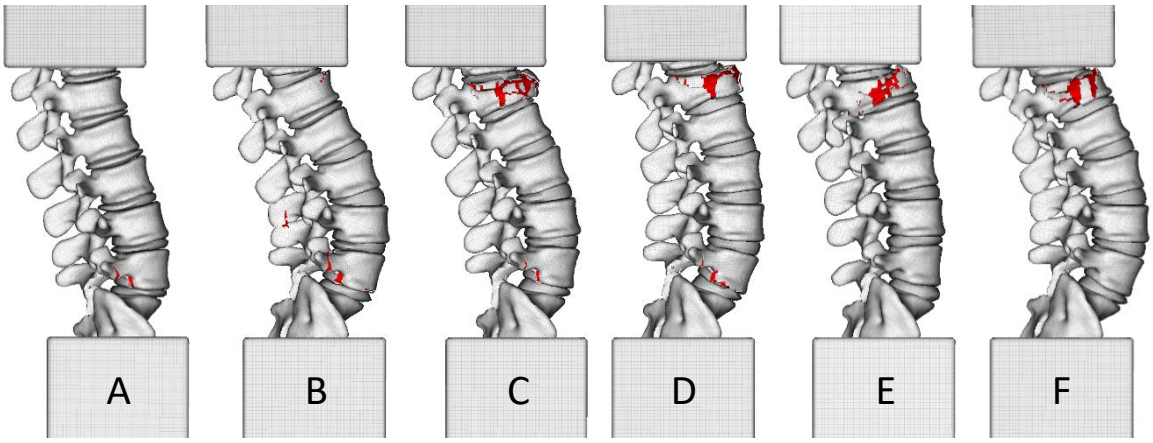

Fig. 5. Comparison of injury location and severity for all six test postures at simulation time 11 ms. Fracture locations are highlighted in red, revealing locations of element deletion within the cortical bone layer. The loading condition for all six tests was identical with a peak velocity of 4.8 m/s, the only change being the posture.

IV. DISCUSSION

At sub-injurious loading, the CAVEMAN lumbar spine was found to perform within ±1 standard deviation of the mean PMHS response through initial peak impact for all postures tested. The six configurations tested with the CAVEMAN spine demonstrated a similar degree of spine compression. Loads at T12 of the CAVEMAN spine were found to display a single peak in the load curve, as opposed to the double peak behaviour observed in the PMHS data. This may be attributed to the material choice in the intervertebral discs lessening the rebound effect after the initial impact. The inclusion of rate-dependent properties in the intervertebral discs may further improve the initial impact response of the model.

The load cell output across non-injurious load simulations of the six postures illustrates a link between lumbar posture and force transmission during vertical loading of the spine, both in the magnitude of peak force and the length of time required to reach peak force. This is in agreement with work in the literature indicating a sensitivity of lumbar spine loading to spine lordosis [25]. Sacrum angle was the dominant factor in load response for these

cases. Posture A had the smallest superior endplate angle from horizontal at -4.7° and experienced the highest magnitude load cell response of the six simulations. The next closest sacrum angle was that of Posture C at -10.4° which experienced the second highest load cell response. The remaining four postures, with sacrum endplate angles ranging from -20.1° to -26.1°, were close in peak force magnitudes, and variations among the load response of this group may be further accounted for in differences between L1-L5 angles across postures.

At injurious input levels, the location of fracture and the degree of lumbar flexion load were found to vary with changes to spine posture and differences in vertebral angles. Fracture of the L1 vertebrae was found to occur as a result of positive moments about the y-axis, with fractures occurring for cases where the moment about the lower load cell exceeded 50 Nm. However no clear trend was observed linking load cell response and fracture of L5 across the six postures. Together, these results illustrate the utility of accounting for variation in spine curvature when validating computational spine models against an experimental data set. As changes in lumbar posture and extension have been linked not just with position (seated versus standing) [26], but also to reported degree of lower back pain in U.S. Marines [27], variation of lumbar angle within a simulation set is more likely to better capture the probability of injury risk at different levels of the spine for a given loading scenario, such as an IED underbody blast event.

The CAVEMAN lumbar spine response was evaluated as it relates to the analysis of injury risk resulting from vertical loading such as occurs in underbody blast events rather than on a subsystem level. For this reason, the model validation sets presented were limited to PMHS whole lumbar experimental data which aimed to replicate these loading conditions. Additional validation of the model at the segment and subsystem level will be done in future studies. Injury analysis is presented here only as a comparison of the six postures under identical load conditions and does not take into account additional factors such as differences in age, bone density, or size of PMHS subjects. It should also be noted that the connective ligaments and musculature of the spine were not included in this model representation which could influence fracture location and severity during *in vivo* loading events.

In this study only variation in posture was considered as a variable parameter. In the experimental environment, such variation in posture can be the result of physical limitations in the PMHS spine to achieve the desired orientation and could potentially lead to a pre-stressed state in the surrounding tissue as the spine is repositioned. The effects of such a pre-stressed state were not evaluated in this work, however it is possible that the influence of a varied initial stress state in the connective regions of the spine could influence the impact response of the spine and, in turn, the type and severity of fractures observed.

V. CONCLUSIONS

The CAVEMAN lumbar spine model demonstrated a biofidelic response that performed within the range of PMHS output across six postures representing variations approximate to the mounted position of the PMHS spine alignment used in the validation test set. Sacrum angle was found to be the main parameter contributing to variation in measured load cell output across the six postures simulated, with shallow potting angles contributing to higher load transmission and earlier occurrence of peak load to the spinal column. When possible, it is recommended to take PMHS curvatures within a validation data set into account during model validation as it may contribute not only an improved understanding of the range of output in an experimental data set but also fewer outliers in the output of the finite element model. Changes in the lumbar posture were also found to influence predicted injury location and severity within the CAVEMAN spine. Consideration of statistical variance in occupant lumbar posture may be an important parameter in future assessment of injury risk and location during vertical loading of the lumbar spine.

VI. ACKNOWLEDGEMENT

This material is based upon work supported by the US Army Research Laboratory (ARL) under Contract No. W911QX-17-C-0029. Any opinions, findings and conclusions or recommendations expressed in this material are those of the authors and do not necessarily reflect the views of the US Army Research Laboratory (ARL).

VII. REFERENCES

[1] Bir C, Barbir A, Dosquet F, Wilhelm M, van der Horst M, Wolfe G. Validation of lower limb surrogates as injury assessment tools in floor impacts due to anti-vehicular land mines. *Military Medicine*, 2008, 173(12):1180-1184.

[2] Iwanoto M, Kisanuki Y, Watanabe I, Furusu K, Miki K, Hasegawa J. Development of a finite element model of the total human model for safety (THUMS) and application to injury reconstruction. *International Research Council on Biomechanics of Injury*, 2002, Munich, Germany.

[3] Iwamoto M, Nakahira Y, Tamura A, Kimpara H, Watanabe I, Miki K. Development of advanced human models in THUMS. *Proceedings of the 6th European LS-DYNA Users' Conference*, 2007: 47–56.

[4] Maeno T, Hasegawa J. Development of a finite element model of the total human model for safety (THUMS) and application to car-pedestrian impacts. *Proceedings of the 17th International ESV Conference*, 2001: 1–10.

[5] Chawla A, Mukherjee S, Mohan D, Parihar A. Validation of lower extremity model in THUMS. *Proceedings of the IRCOBI Conference*, 2004, Graz, Austria.

[6] Gayzik F, Moreno D, Vavalle N, Rhyne A, Stitzel J. Development of the Global Human Body Models Consortium Mid-Sized Male Full Body Model. *Injury Biomechanics Research*, 2011: 39–12.

[7] Vavalle N, Moreno D, Rhyne A, Stitzel J, Gayzik F. Lateral impact validation of a geometrically accurate full body finite element model for blunt injury prediction. *Annals of Biomedical Engineering,* 2013, 41(3):479–512.

[8] Karajan N. Multiphasic Intervertebral Disc Mechanics: Theory and Application. *Archives of Computational Methods in Engineering,* 2012, 19:261–339.

[9] Schmidt H, Heuer F, Simon U, Kettler A, Rohlmann A, Claes L, Wilke H-J. Application of a new calibration method for a three-dimensional finite element model of a human lumbar annulus fibrosus. *Clinical Biomechanics,* 2006, 21(4):337–344.

[10] Kingma I, van Dieën J H, Nicolay K, Maat J, Weinans H. Monitoring water content in deforming intervertebral disc tissue by finite element analysis of MRI data. *Magnetic Resonance in Medicine,* 2000, 44(June 1999):650–654.

[11] Naserkhaki S, Jaremko J L, Adeeb S, El-Rich M. On the load-sharing along the ligamentous lumbosacral spine in flexed and extended postures: Finite element study. *Journal of Biomechanics,* 2016, 49(6):974–982.

[12] Dreischarf M, Zander T, Shirazi-Adl A, Puttlitz C M, Adam C J, Chen C S, Goel V K, Kiapour A, Kim Y H, Labus K M, Little J P, Park W M, Wang Y H, Wilke H J, Rohlmann A, Schmidt H. Comparison of eight published static finite element models of the intact lumbar spine: Predictive power of models improves when combined together. *Journal of Biomechanics,* 2014, 47(8):1757–1766.

[13] Shirazi-Adl A. Analysis of large compression loads on lumbar spine in flexion and in torsion using a novel wrapping element. *Journal of Biomechanics,* 2006, 39(2):267–275.

[14] El-Rich M, Arnoux P J, Wagnac E, Brunet C, Aubin C E. Finite element investigation of the loading rate effect on the spinal load-sharing changes under impact conditions. *Journal of Biomechanics,* 2009, 42(9):1252–1262.

[15] Zanjani-Pour S, Winlove C P, Smith C W, Meakin J R. Image driven subject-specific finite element models of spinal biomechanics. *Journal of Biomechanics,* 2016, 49(6):919–925.

[16] Jones A C, Wilcox R K. Finite element analysis of the spine: Towards a framework of verification, validation and sensitivity analysis. *Medical Engineering and Physics,* 2008, 30(10):1287–1304.

[17] Butz K, Spurlock C, Roy R, Bell C, Barrett P, Ward A, Xiao X, Shirley A, Welch C, Lister K. Development of the CAVEMAN Human Body Model: Validation of Lower Extremity Sub-Injurious Response to Vertical Accelerative Loading. *Stapp Car Crash Journal,* 2017, 61.

[18] Yoganandan N, Zhang J, Moore J, Pintar F, Baisden J L. Lumbar Spinal Column Injuries and Loads from Inferior-to-Superior Impact: Applications to Military and Automotive Environments. *IRCOBI Asia 2018*, 2018:70–71.

[19] Gibson M W, Armiger R S, Biermann P J, Boyle M P, Iwaskiw A S, Lennon A M, Merkle A C, Pyles C O, Seker D P, Vavalle N A, Xia Z, Zhang J, Crawford D M, Chowdhury M R. Warrior Injury Assessment Manikin (WIAMan) Lumbar Spine Model Validation: Development, Testing, and Analysis of Physical and Computational Models of the WIAMan Lumbar Spine Materials Demonstrator, 2016, https://apps.dtic.mil/docs/citations/AD1013367.

[20] Weiss J A, Maker B N, Govindjee S. Finite element implementation of incompressible, transversely isotropic

hyperelasticity. *Computer Methods in Applied Mechanics and Engineering,* 1996, 135(1–2):107–128.
[21] Elliott D M, Setton L A. A linear material model for fiber-induced anisotropy of the anulus fibrosus. *Journal of Biomechanical Engineering,* 2000, 122(April 2000):173–179.
[22] Iatridis J C, Setton L A, Foster R J, Rawlins B A, Weidenbaum M, Mow V C. Degeneration affects the anisotropic and nonlinear behaviors of human anulus fibrosus in compression. *Journal of Biomechanics,* 1998, 31:535–544.
[23] Kopperdahl D L, Keaveny T M. Yield strain behavior of trabecular bone. *Journal of Biomechanics,* 1998, 31(7):601–608.
[24] Shirazi-Adl A, Ahmed A M, Shrivastava S C. Mechanical response of a lumbar motion segment in axial torque alone and combined with compression. *Spine,* 1986, 11:914–927.
[25] Putzer M, Ehrlich I, Rasmussen J, Gebbeken N, Dendorfer S. Sensitivity of lumbar spine loading to anatomical parameters. *Journal of Biomechanics,* 2016, 49(6):953–958.
[26] Hey H W D, Lau E T-C, Tan K-A, Lim J L, Choong D, Lau L-L, Liu K-P G, Wong H-K. Lumbar Spine Alignment in Six Common Postures. *Spine,* 2017, 42(19):1447–1455.
[27] Berry D B, Rodríguez-Soto A E, Su J, Gombatto S P, Shahidi B, Palombo L, Chung C, Jensen A, Kelly K R, Ward S R. Lumbar spine postures in Marines during simulated operational positions. *Journal of Orthopaedic Research,* 2017, 35(10):2145–2153.